#### ORIGINAL RESEARCH



# Using interfacial behavior and adsorption kinetics measurements as a predictor of bulk hydrophobic development of paper supercritically impregnated with food-grade waxes

Brenda Helen Hutton-Prager · Joseph P. Fallon · Blake Henke · Raymond Zhang · Withanage Keshani Rangika Perera

Received: 16 March 2024 / Accepted: 24 June 2024 / Published online: 2 July 2024 © The Author(s) 2024

Abstract Supercritical Impregnation methods are becoming popular in the development of food packaging materials. Bulk functional improvements of cellulose substrates using this method may be influenced by interfacial interactions between the impregnated solutes and cellulose. Hence, an interfacial adsorption kinetics study of solute molecules onto the substrate can provide insight on bulk property development, leading to an optimized packaging material with improved functionality. Paper substrates were impregnated with two food-grade waxes: Alkyl Ketene Dimer (AKD) and Carnauba Wax (CW). Hydrophobic development was monitored over a 3-week period. A quartz crystal microbalance (QCM-D) was used to determine interfacial characteristics and behavior of

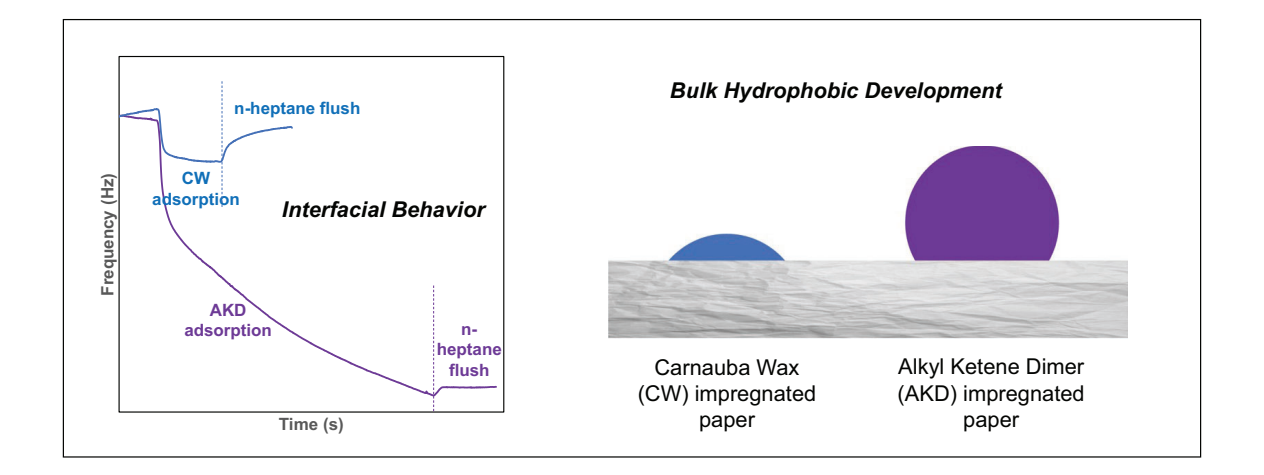
each wax with cellulose, and adsorption kinetics were quantified to compare the mass transfer processes of each wax at the interface. AKD significantly contributed to the substrate's hydrophobic development over time. CW generated mildly hydrophobic substrates only when heated. AKD strongly adhered to the cellulose fibers at the interface, and demonstrated a 3-stage kinetic adsorption process, tentatively assigned (i) diffusion through the substrate; and (iii) attachment onto the fibers. CW readily washed off the cellulose surface, demonstrating only the first adsorption process. The different chemical structures also impacted these behaviors, as did concentration and temperature.

**Supplementary Information** The online version contains supplementary material available at https://doi.org/10.1007/s10570-024-06032-2.

B. H. Hutton-Prager (□) · J. P. Fallon · B. Henke · R. Zhang · W. K. R. Perera
Department of Chemical Engineering, University of Mississippi, University, MS 38677, USA e-mail: bhprager@olemiss.edu



# **Graphical Abstract**



**Keywords** Quartz Crystal Microbalance · Adsorption kinetics · Interfaces · Cellulose · Supercritical impregnation · Hydrophobicity

#### Introduction

Food packaging, and packaging in general, has become a popular area of research and development as the demand for sustainable and recyclable packaging continues to gain momentum (Nechita and Roman (2020); Wang et al. 2022). Paper packaging has long been the preference due to its innate abilities to decompose in landfill, however as coatings applied to paper become more functional and multi-purpose, it is necessary to ensure that these too are sustainable to aid in the recycling efforts.

One of many important functions for packaging is to repel water, and hence improving the hydrophobicity of paper is necessary for paper-based packaging, given the inherent hydrophilicity of cellulosic fibers. During papermaking, alkyl ketene dimer (AKD) dispersed in cationic modified starch is often introduced at the wet end to impart a sizing effect (Kumar et al. 2016). Traditional methods of hydrophobizing paper after its production include surface sizing with starch (Teixeira Moutinho et al. 2009); coatings with waxes or oily polymers laminated onto the substrate (Nechita and Roman (2020)); petroleum-based waxes (Nechita and Roman (2020)); and 'traditional' coating formulations consisting of a mineral pigment and

dispersing agent, polymeric binder, and small quantities of additives that can be chosen to impart a particular barrier property (Lambourne and Strivens 1999; Di Risio and Yan 2006; Tracton 2007; Hutton and Parker 2008; Brock et al. 2010; Howard and Hodgson 2015). Many of these methods are not particularly conducive to recyclability efforts.

More novel methods gaining momentum are those employing supercritical fluids (SCF), often carbon dioxide (scCO<sub>2</sub>) at either sub- or supercritical pressures. Supercritical impregnation (SCI) involves dissolving a hydrophobic wax such as AKD or foodgrade wax into the SCF, often using small quantities of organic cosolvent, and then impregnating the wax into the paper substrate. Subsequent depressurization of the system causes the SCF to return to gaseous state, leaving the waxy solid impregnated into the fiber network (Hutton-Prager et al. 2021). Other methods include rapid expansion of a supercritical solvent (RESS) (Quan et al. 2009; Misra and Pathak 2020; Kumar et al. 2021) and supercritical antisolvent (SAS) methods (Rossmann et al. 2013; Misra and Pathak 2020; Franco and De Marco 2020; Santos et al. 2022). Various examples include those reviewed by Kiran (Kiran 2016); the Werner and Quan group (Quan et al. 2009; Werner et al. 2010; Werner and Turner 2012); and Chen, Song, and Xu (Chen et al. 2018). Our research group has also conducted several such studies using SCI methods (Adenekan and Hutton-Prager 2019, 2020; Hutton-Prager et al. 2021; Beheshtimaal and Hutton-Prager 2022). Although



not formally tested, the reverse process, supercritical extraction (SCE), ideally can extract the waxes from waste packaging back into the SCF and hence remove the solute, enabling a realistic possibility for recyclability of these types of papers.

Chemical modification using long-chain hydro-carbon-based molecules is well-known to improve the hydrophobicity of a substrate as it increases the water-droplet surface contact angle (CA). This CA can also be greatly increased by roughness and porosity of the substrate under certain conditions, and hence physical characteristics of the substrate are also important. Young's equation describes the CA ( $\theta$ ) between a liquid and solid surface, and is a balance of forces or energy (mNm<sup>-1</sup>) between the solid–vapor phase ( $\sigma_{SV}$ ), the solid–liquid phase ( $\sigma_{SL}$ ), and the liquid–vapor phase ( $\sigma_{LV}$ ):

$$\sigma_{SV} = \sigma_{SL} + \sigma_{LV} cos\theta \tag{1}$$

Equation (1) is valid only for smooth, solid surfaces, and is often modified to the Wenzel equation to introduce roughness, or the Cassie-Baxter equation to introduce roughness and porosity or chemical heterogeneity (Mohamed et al. 2015). Still, fundamentally, Young's equation can be used to predict some broad behaviors arising from a given situation, within reasonable assumptions. The modified equations additionally demonstrate the changes in CA possible by introducing roughness and/or porosity to the substrate.

Despite promising developments both by our research group and others with regard to functionalizing paper using high-pressure technologies, there is a present lack of knowledge regarding the interfacial adsorption behavior of wax molecules onto cellulose fibers. Continued development of sustainable, paperbased packaging centers on enhanced knowledge of the influences of wax attachment to the cellulosic fibers; the strength of these attachments; and the ease with which these waxes may be removed. Wang and Guo (Wang and Guo 2020) extensively reviewed several adsorption kinetics processes that help explain the mass transfer steps taking place, highlighting the importance of assigning physical meaning to various empirical models proposed. The pseudofirst order (PFO, Eq. (2)) and pseudo-second order (PSO, Eq. (3)) models are commonly applied in many analyses despite the limitations of physical meanings to the constants within the models:

$$q_t = q_e \left( 1 - e^{-k_1 t} \right) \tag{2}$$

$$\frac{t}{q_t} = \frac{t}{q_e} + \frac{1}{k_2 q_e^2} \tag{3}$$

In the above equations and as used in subsequent analyses, q represents the adsorbed quantity ( $ngcm^{-2}$ ) at time t (s) or e (equilibrium);  $k_1$  is the first-order rate constant (s<sup>-1</sup>); and  $k_2$  is the second-order rate constant  $(cm^2ng^{-1} s^{-1})$ . Hu, Wang, Feng et al. (Hu et al. 2018) cited special cases of the PFO for the initial adsorption during PSO behavior, showing similarities in the two models at short times after adsorption had begun. Various experimental factors were identified that could influence the kinetics, such as solute concentration, pH, and temperature. The well-known Langmuir isotherm was shown to mimic the PSO form mathematically, leading to equivalencies between the Langmuir constant and  $k_2$ , and hence likely additional influences of temperature on this rate constant. Fang, Zhuang, Huang et al. (Fang et al. 2020) conducted an extensive study into the kinetics models of first-order, second-order, pseudo-first order, and pseudo-second order models. They similarly identified large changes in the rate constants of these models based on initial concentrations, volumes used, and dosages applied.

Adsorption/desorption kinetics studies at the interface of a system may be studied with a Quartz Crystal Microbalance (QCM-D) (Shen et al. 2015; Chen et al. 2016; Dourado et al. 2018; Medina et al. 2020; Cui et al. 2020; Adamczyk et al. 2022). Typical analyses from such studies has included extensive use of the PFO and PSO equations for both adsorption and desorption processes (Shen et al. 2015; Medina et al. 2020), including the use of multiple PFO equations to represent different kinetic stages within a process. The quartz crystal is set to oscillate at multiple overtones or harmonic numbers (n=3, 5, 7, 9, 11, 13) of the base frequency of the crystal, 5.0 MHz ( $f_w$ , n=1). The sensors, connected to the crystal via an electric circuit, become heavier when solute solutions are pumped across their surface, causing the oscillation frequencies to change accordingly. The change in frequency is correlated with the change in mass of the solute directly adsorbed onto the substrate sensor surface, and the rate



at which this occurs can be obtained by measuring the frequency changes with time (Chen et al. 2016).

The overall goal of this study is to explain the development of bulk hydrophobicity in papers supercritically impregnated with food-grade waxes using observed interfacial behavior and adsorption kinetics between the impregnating wax solute and the cellulosic fibers. To do this, three supporting objectives will be explored: a) quantify the bulk hydrophobic development over a three-week period of paper substrates supercritically impregnated with AKD and Yellow Carnauba Wax (CW) using scCO2 (both food-grade or approved for use in food packaging by the FDA (2024a, b)); b) determine the interfacial characteristics between each of the waxes and cellulose fibers via a QCM-D study; and c) model and compare the adsorption kinetics of each wax onto the cellulose fibers. The first objective will enable the hydrophobic development to be compared between the two waxes, while the second will identify the different behaviors of each wax with regard to their bonding behavior onto the cellulose fibers. The final objective aims to quantify the various stages involved in solute mass transfer during adsorption, and again will compare any differences between the two waxes during this process. This investigation uses pure cellulose to represent paper substrates for the bulk studies, and cellulose nanocrystals (CNCs) to represent paper in the interfacial studies, both of which are not fully representative of paper-based substrates used in packaging. Results are somewhat idealistic in the sense that identified interactions of solutes with cellulose are in the absence of other agents incorporated into manufactured paper substrates (e.g. wet strength and internal sizing agents, bleaching chemicals). Should this work progress to production scale, more complex and realistic systems will be investigated.

## Materials and methods

#### Materials

AKD (Aquapel<sup>TM</sup> 364 K sizing agent) with chain lengths C16 to C18, and CW (Koster Keunen) were the waxes used to investigate interfacial interactions between themselves and cellulose fibers. Each was prepared as a 1.8 g/L solution in n-heptane (99%, Sigma Aldrich), and diluted for studies at lower concentrations. A 1 wt% dispersion of cellulose

nanocrystals (CNCs, USDA forest products laboratory, University of Maine) in deionized (DI) water (Direct-Q 3UV system) was prepared to spin-coat QSense silicon dioxide (SiO<sub>2</sub>) sensors (QSX 303). Although only the crystalized form of cellulose, it was used to chemically represent cellulose for the interfacial studies. Two cleaning fluids for the QCM-D were prepared as 2% w/w in DI water, and consisted of sodium dodecyl sulphate (SDS, Sigma-Alrdich), and Hellmanex III (Sigma Aldrich). Compressed nitrogen (nexAir) was used to dry QCM-D components and operate the spin-coater. Supercritical fluid (SCF) grade carbon dioxide was provided by Airgas USA, LLC. Whatman 1 filter paper, 110 mm diameter (Sigma Aldrich) was used as a paper substrate for the supercritical experiments. This is a near pure form of cellulose, made from cotton lint fibers.

#### Methods

## SCI experiments

Impregnation experiments were performed on a SCI rig built in-house and described elsewhere (Adenekan and Hutton-Prager 2019; Hutton-Prager et al. 2021; Beheshtimaal and Hutton-Prager 2022). Briefly, 6 mL of wax at 1.8 g/L was inserted into a vessel and subsequently dissolved in scCO<sub>2</sub> (T=20 °C, P=200 bar, i.e. supercritical in pressure but not temperature) for 10 min by pumping the contents around a circulating loop. After this time, the combined fluid was sent to a second vessel that contained two strips of Whatman 1 filter paper (6 mm × 80 mm), and the wax was allowed to impregnate this paper for 15 min. Upon depressurization of the contents, the paper was collected for subsequent analyses. Some strips were annealed in a 1300 W oven (Precision Scientific Inc. Division, Winchester, Virginia) for 4 h at 140 °C, while others were stored at room temperature. Both annealed and non-annealed papers were analyzed on Days 1, 7, 14, and 21, for hydrophobic development (i.e. CA measurements) and microscopic imaging.

#### CA Measurements

A Biolin OneAttension CA Analyzer was used to take sessile and pendant drop measurements. Sessile drops were used to assess the hydrophobic development of the impregnated paper, and 10  $\mu$ L droplets of DI



water were placed on the surface with the CA being subsequently monitored until full penetration (usually several minutes). These measurements were repeated in triplicate, and over different days (Day 1, 7, 14, 21), with typical standard deviations between repeats falling within ±5°. Similar sessile measurement procedures were also conducted using wax/heptane solutions on CNCs-coated sensors to determine the CA of the wax droplets on cellulose. Pendant drop measurements were performed to determine the surface tension of each wax/heptane solution. In these measurements, the largest drop prior to exiting the syringe tip was generated, and the curvature was recorded for 10 s. These were also prepared in triplicate and averaged.

## Digital imaging

A Keyence microscope (VHX7000) was used to take images of the impregnated paper on Days 1, 7, 14, 21, to match its hydrophobic development with the corresponding CA measurements. Images were taken over a variety of magnifications ( $\times 20, \times 100, \times 200$ ).

## QCM-D experiments

A Q-Sense Analyzer, 4-channel QCM-D System (Biolin Scientific-NanoScience) was used to assess the adsorption behavior of the waxes onto the cellulose molecules. Flow modules (QFM401) were initially cleaned at 30 °C by flushing 10 mL of n-heptane per module at 0.3 mL/min, followed by air. The modules were then dried in nitrogen. Meanwhile, Q-Sense SiO<sub>2</sub> sensors (QSX303) were pre-cleaned using the following procedure: 10 min of UV/ozone treatment; 30 min in 2% w/w SDS solution at approx. 50 °C; DI water rinse; nitrogen drying; 10 min of UV/ozone treatment. A spincoater (WS-650\_BT Series, Laurell Technologies) was used to coat each sensor with 1 wt% CNCs dispersion. Using static mode, 3 droplets of dispersion were placed on the sensor followed by the static drying regime (performed twice) and the speed test (performed once). Sensors were left to dry beneath an upturned beaker for two hours prior to starting the adsorption experiment. Interfacial experiments were conducted at 20 and 30 °C, and a 5 s average of data collection was used. The wax/heptane solutions were pumped through the modules at 0.1 mL/

min. A solvent baseline was established by flushing n-heptane through the modules, followed by the wax/n-heptane solution of interest. Upon equilibration, more n-heptane was flushed through the system to determine the strength of wax attachment to the cellulose fibers. Once the experiment was completed, the modules were again flushed with n-heptane and air, then dried in nitrogen, while the contaminated SiO<sub>2</sub> sensors underwent a different cleaning regime from the pre-experiment procedure: 10 min UV/ozone treatment; 10 min in 2% w/w Helmanex solution at approx. 50 °C; 10 min in DI water at 50 °C; nitrogen drying; 10 min UV/ ozone treatment. The sensors were placed back into the module to test their dissipation and amplitude signals to confirm that the cleaning method was acceptable before reuse.

## Adsorption kinetic modeling studies

The change in frequency values of the  $f_7$  overtone signal were converted to a change in mass value using the Sauerbrey equation as given in Eq. (4) (Medina et al. 2020). Data were subsequently adjusted to start at time t=0 for each section of interest. Where necessary, large quantities of data were reduced by selecting every 2nd to 7th data point such that

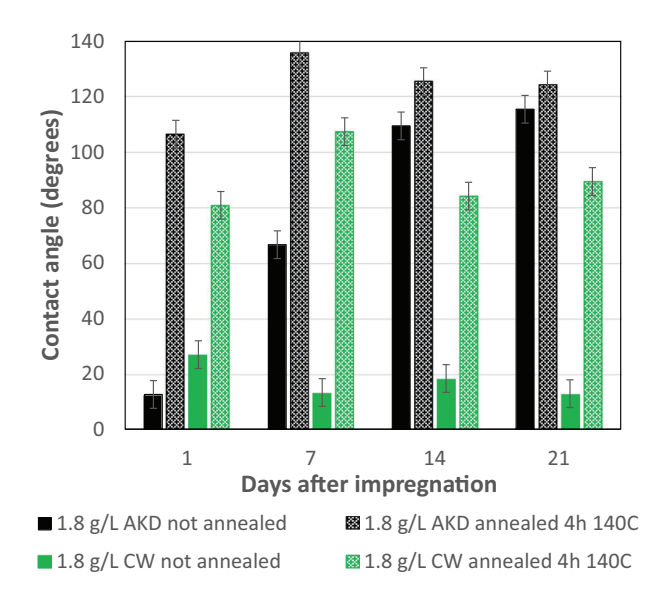


**Fig. 1** Contact angle of wax-treated paper for AKD and CW over a three-week period, showing results for both annealed (4 h, 140 °C) and non-annealed samples



approximately 100 data points remained for analysis. Excel Solver (Microsoft Office Professional Plus 2019) was employed to fit these data points using single or multiple PFO kinetics, and PSO kinetics, as described in Eqs. (2) and (3), respectively (Wang and Guo 2020). Standard deviations (SD) for each section were calculated by the sum of squares method (Fang et al. 2020), and then compared to choose the best kinetic fit. Finally, fitted constants were compared amongst experimental conditions and discussed.

#### Results and discussion

Hydrophobic development of paper substrates impregnated with waxes

CA measurements were conducted on the Whatman paper substrates impregnated with AKD or CW over a three-week period to quantify hydrophobic development with time, and results are shown in Fig. 1. AKD-treated paper generally had higher CA than CW-treated paper, and by Day 14, the

non-annealed samples showed similar hydrophobicity to the annealed samples. AKD is known to take approximately two weeks to fully develop its sizing effect on paper substrates without the assistance of heat energy (Adenekan and Hutton-Prager 2019; Beheshtimaal and Hutton-Prager 2022), but with annealing, adequate sizing was achieved from Day 1. Annealing was found necessary to give CW-treated paper a somewhat hydrophobic effect throughout the entire time period (most samples were 'almost' hydrophobic, with CA just below the theoretical 90° value). Without annealing, the impregnation of CW did not provide substantial improvements to paper hydrophobicity, with most results being below 20°. Similar behavior has been observed previously with other food-grade waxes (Hutton-Prager et al. 2021; Beheshtimaal and Hutton-Prager 2022) where heating was found necessary to develop a sizing effect. With impure waxes particularly, annealing is believed to cause polymorphic phase separation of the wax components and subsequent regrouping or redistribution, often resulting in a changed morphological surface with enhanced nano-/micro-structures. This

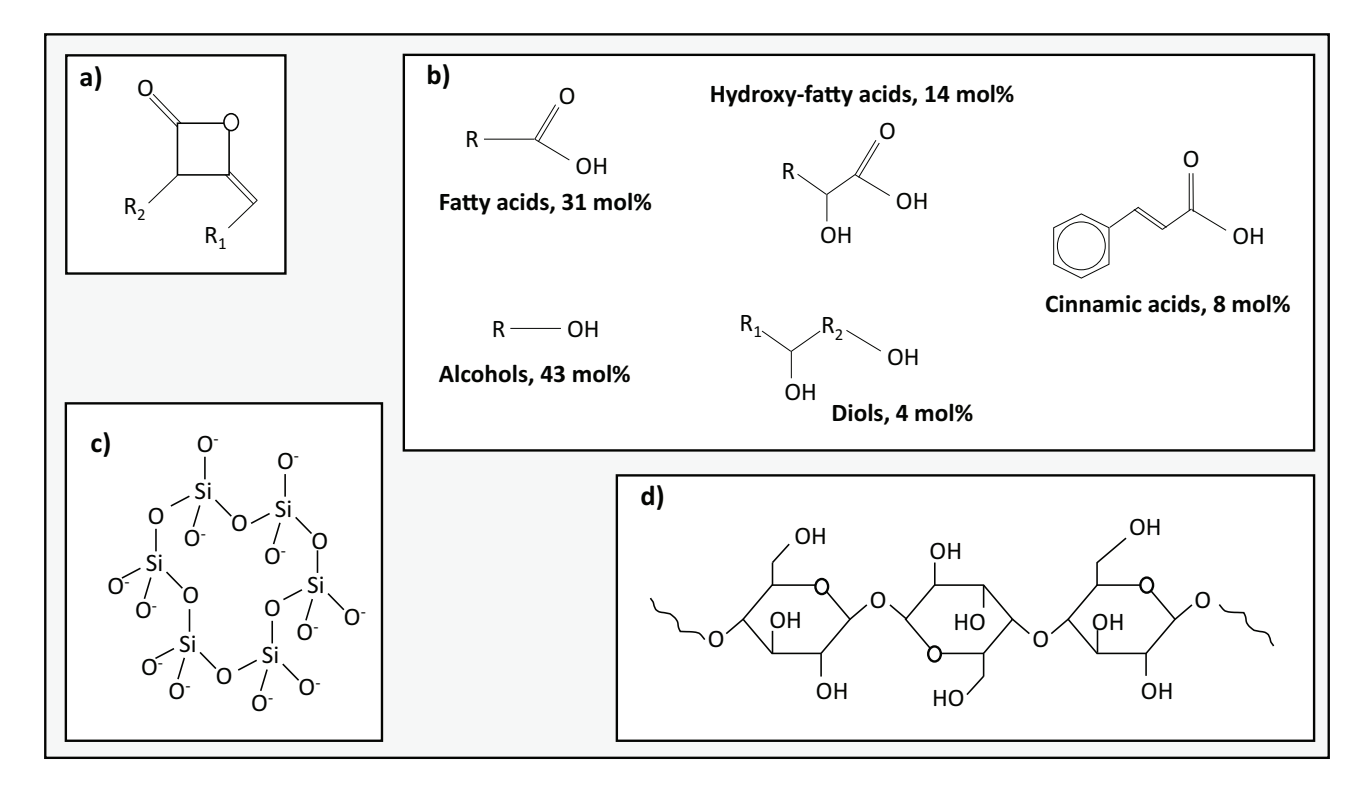


**Fig. 2** a AKD, with  $R_1$  and  $R_2$  between  $C_{16} - C_{18}$ ; **b** different structures making up CW, together with average molar composition, where  $R = R_1 + R_2$ , and R is between  $C_{16} - C_{32}$  (Wang

et al. 2001);  $\bf c$  substrate structure of  ${\rm SiO_2}$  which is the uncoated Qsense sensor surface;  $\bf d$  substrate structure of cellulose, which was coated onto the  ${\rm SiO_2}$  sensors



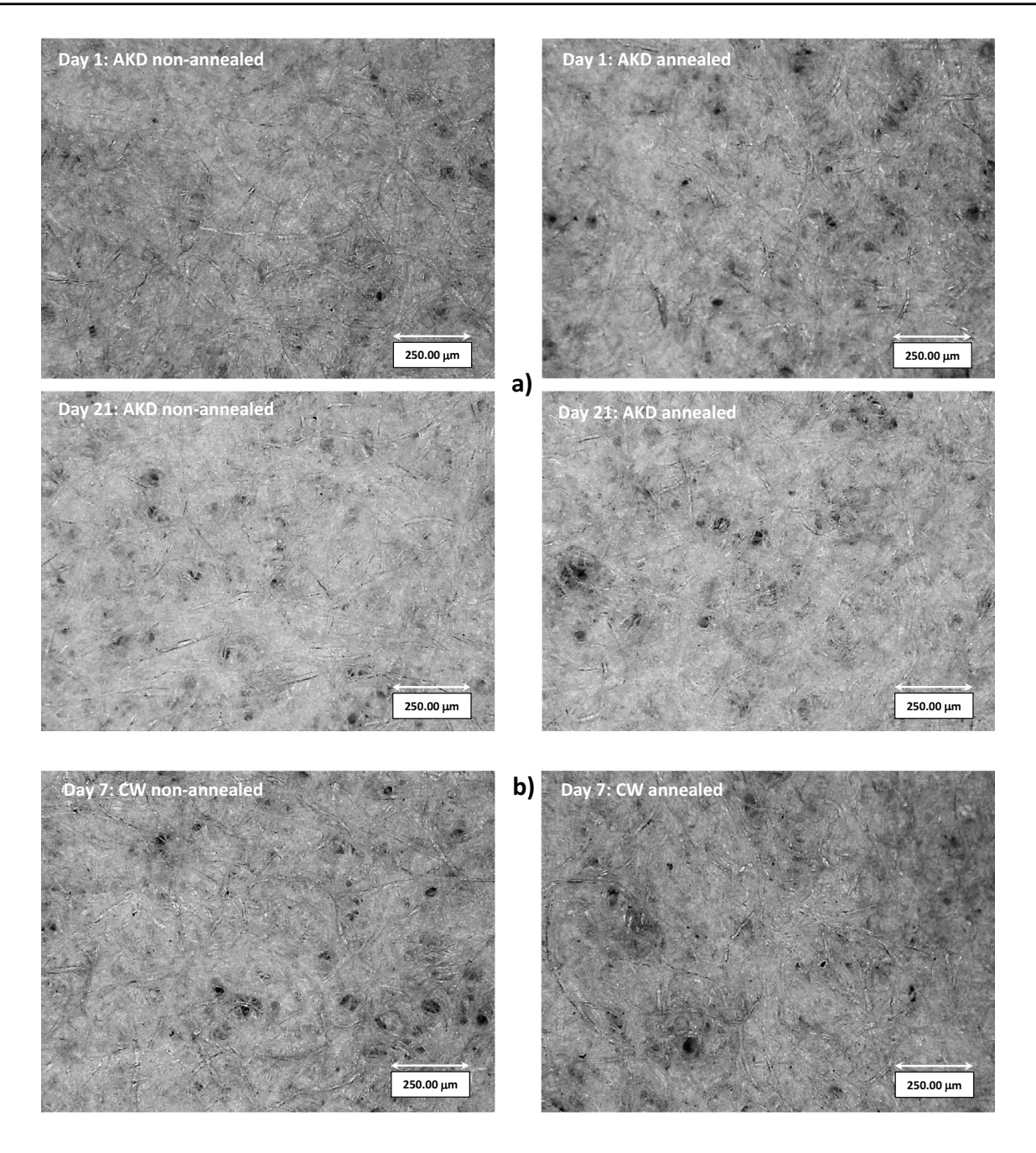


**Fig. 3** a AKD-treated paper on Day 1 (top) and 21 (bottom), comparing non-annealed paper on the left with annealed paper on the right (4 h 140 °C, immediately after impregnation). **b** 

CW-treated paper on Day 7, non-annealed (left) and annealed (right) at the same conditions as  $AKD\,$ 

additional structure typically favors higher CA of water droplets applied to the surface (Zhang et al. 2014). Despite both waxes containing significant hydrocarbon content (see Fig. 2a and b), the different wax structures and the multi-component CW compound (Wang et al. 2001; Puttalingamma 2014) may have impacted the way these molecules attached to the cellulose. Previous work by the authors

(Adenekan and Hutton-Prager 2019) has shown that AKD H-bonds to the -OH groups on cellulose molecules via its=O and/or the -O- groups. This enables the two R-groups to point outwards from the cellulose substrate and provide hydrophobic modification to the cellulose. The annealing treatment appears to speed up this process. The individual components within CW can also H-bond to the cellulose via=O bonds



in some fractions and -OH groups in other fractions. However, many of these potential H-bonding opportunities may already be occurring between the CW fractions, and structural hindrance of the different fractions may prevent full access to the available -OH groups on the cellulose. Consequently, from a purely structural viewpoint, it is logical to assume that CW may not attach to the cellulose as easily as AKD. The annealing step can allow a freeing up of the individual fractions from each other, and rearrangement of these fractions may enable higher attachment probabilities, thereby improving the resulting hydrophobicity observed.

The impregnated paper samples were imaged with a Keyence microscope on the same days as the CA measurements over the three-week period (Days 1, 7, 14, 21). From Fig. 1, it is known that the AKDimpregnated paper resulted in similar CA from Day 14 onwards for both annealed and non-annealed samples. This result is supported with spatial observations shown in Fig. 3a. In these images: (i) there is less fiber coverage of AKD on the non-annealed sample, Day 1, compared with the annealed sample; and (ii) Day 21 shows similar fiber coverage irrespective of the heat treatment performed. These observations are also consistent with many descriptions of AKD 'spreading' over the fibers with time (Adenekan and Hutton-Prager 2019; Beheshtimaal and Hutton-Prager 2022), seen by more fiber coverage at Day 21

compared with Day 1 for the non-annealed samples. Both annealed samples on different days look alike, confirming the more rapid sizing effect from the heat treatment resulting in similar CA. The nano-/micro-structural changes in annealed samples referred to earlier are not observed with these images due to the lower magnifications used – these magnifications were necessary to observe the AKD spreading behavior.

Spatial comparisons were also conducted for CW, however different observations became apparent. As per Fig. 1, the CA was similar over the three-week period for non-annealed samples (average 18°) and annealed samples (average 90°). The images were correspondingly similar over this time period for each group (i.e. non-annealed and annealed). Unexpectedly, at any given time, the images were also quite similar between non-annealed and annealed conditions, despite the vast differences in measured CA, depicted in Fig. 3b for Day 7. This change in CA is likely due to the development of nano-/microstructural surface changes observed in earlier works (Hutton-Prager et al. 2021; Beheshtimaal and Hutton-Prager 2022), while the spreading phenomenon with time was not dominant. There are insufficient studies in the literature regarding similar spreading observations for CW compared with those describing the common spreading behavior for AKD.

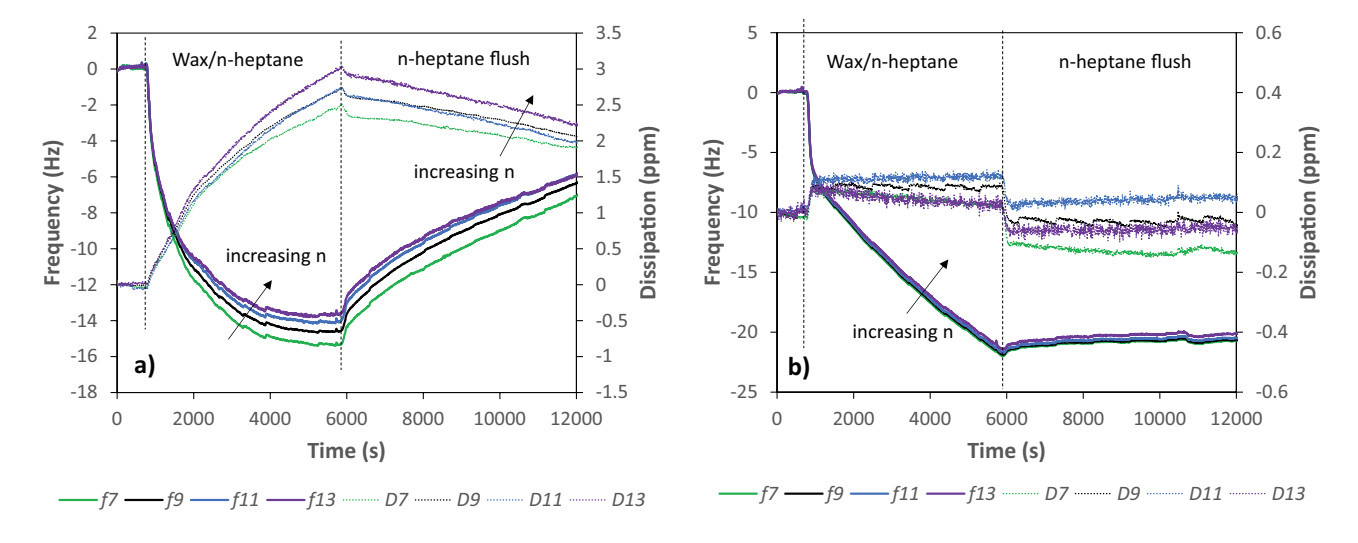


Fig. 4 0.9 g/L AKD/heptane pumped through the system at 30 °C, over a SiO<sub>2</sub> sensors and b SiO<sub>2</sub> sensors, spin-coated with 1 wt% CNCs. Adsorption and flushing sections are identified



Interfacial behavior between waxes and cellulose using the QCM-D

## Viscous nature of the adsorbed layers

Irrespective of wax, wax concentration, and temperature, the raw data frequency curves collected at multiple overtones (n=7, 9, 11, 13) of the quartz crystal vibrations closely overlapped each other. The lower overtones (n=3 and 5) were at times noisy, but had settled by n=7 across all conditions tested. Consequently, the resulting wax layers were described as rigid, thereby establishing Sauerbrey behavior according to Eq. (4) (Fang et al. 2020; Easley et al. 2022):

$$\Delta m = \frac{-C}{n} \Delta f \tag{4}$$

The above equation allows for a simple conversion from the change in frequency between the baseline and the curve ( $\Delta f$ , Hz) to a change in mass ( $\Delta m$ , ngcm<sup>-2</sup>). The mass sensitivity constant of the sensor, C, is often assigned a value of 17.8 ngcm<sup>-2</sup> Hz<sup>-1</sup> (Fang et al. 2020). The change in dissipation ( $\Delta D$ ) from the baseline in all cases was very low, and mostly below 0.2 ppm, indicating that a recordable dissipation response was not achieved (Easley et al. 2022). Such small changes in  $\Delta D$  are also indicative of rigid layers forming on the sensors. The AKD studies showed that with higher AKD/n-heptane

concentrations, the  $\Delta D$  curves gradually increased, however response signals were still too low to draw conclusions other than rigid layer formations.

# Effect of substrate

In one experiment, 0.9 g/L AKD wax at 30 °C was pumped across uncoated SiO2 sensors, and was compared with an identical trial using sensors spin-coated with 1 wt% CNCs (Fig. 4). For the uncoated sensors, both  $\Delta f$  and  $\Delta D$  curves did not overlap; both showed increases in value with increasing n; and the  $\Delta D$ curves were well into the experimental response range (i.e.>0.2 ppm). Many of these observations indicate viscoelastic layers forming on the sensors (Easley et al. 2022). The AKD deposits stabilized at approximately 6000 s on the uncoated sensors and were slowly washed off during the heptane flush. The experiment using CNCs-coated sensors showed that the AKD adsorption did not stabilize after a long time, but subsequent flushing with heptane removed very little wax, as it was firmly attached to the sensors. Since the cellulose coating was the only difference between the two experiments, it appears to be responsible for minimizing dissipation; anchoring the wax firmly in place to form rigid layers; and promoting hydrogen bonding between the wax and cellulose molecules.

The uncoated SiO<sub>2</sub> sensors and 1 wt% CNCs-coated sensors provided vastly different surfaces (and hence interfaces) in contact with the AKD molecules.

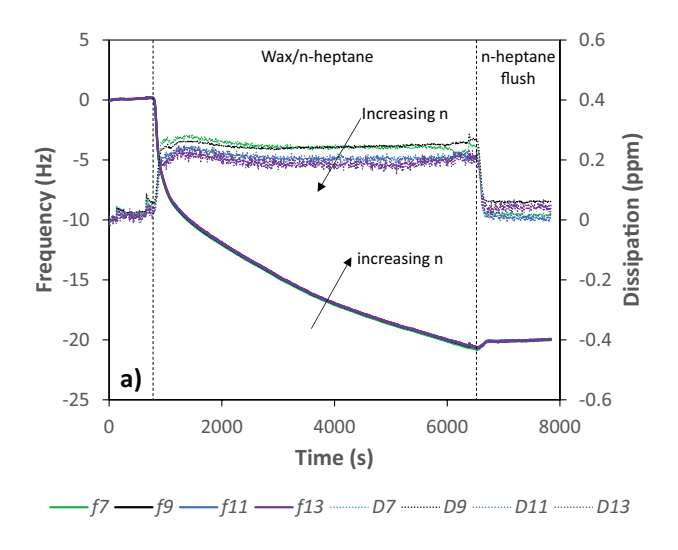
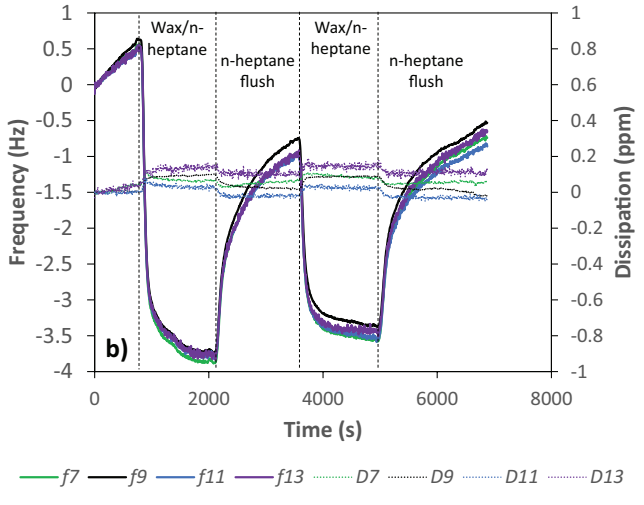


**Fig. 5 a** AKD and **b** CW adsorption onto cellulose-coated sensors, performed at 20 °C and 1.8 g/L wax/heptane concentration. Also observed in this figure is the closely overlap-



ping  $\Delta f$  and  $\Delta D$  curves, indicating rigid adsorbed wax layers. Adsorption and flushing sections are identified



Cellulose is a biopolymeric network with many -OH groups that enable H-bonding with AKD, while SiO<sub>2</sub>, or essentially silica, is a giant molecule consisting of many Si and O atoms covalently bonded together (Fig. 2c and 2d). The=O and -O- structures in the AKD ring repel the highly electronegative oxygen atoms bonded to the silicon atoms. Despite the same concentration of AKD/n-heptane used in this comparison, the CNCs-coated sensors provided higher selectivity and compatible surface characteristics with AKD than the SiO<sub>2</sub> sensors, resulting in higher  $|\Delta f|$ values and low removal during n-heptane flushing. Conversely, the lower compatibility of the SiO<sub>2</sub> sensors with AKD resulted in less partitioning of AKD towards this substrate and hence lower  $|\Delta f|$  value) and easy removal of the wax during the n-heptane flush.

# Effects of wax structure

The QCM-D results for AKD and CW at 20 °C are shown in Fig. 5 at constant concentration of 1.8 g/L of wax/heptane solution. Very different adsorption kinetic behavior is observed (note shape of the  $\Delta f$  curves). Both show an immediate drop in frequency, however the AKD takes a very long time to stabilize whereas the CW comes to equilibrium quite quickly, and hence a second cycle of wax adsorption and flushing was performed. The n-heptane flush sequences demonstrated that almost no AKD is washed off the cellulose surface whereas 65% of the CW on average, is washed off (based on the change in  $\Delta f$  values). The other notable observation is that despite the concentration of each wax being identical, vastly different  $\Delta f$  values were recorded for each wax. AKD had reached a value of -21 Hz before starting the n-heptane flush, whereas CW had reached -4.5 Hz. One likely reason for this is that the CW tended to form a suspension in the n-heptane rather than a solution at this concentration, although only a very small amount of wax remained undissolved. The saturated solution pumped over the sensor surface was subsequently at slightly less than 1.8 g/L, but was not expected to be solely responsible for the observed dramatic change in  $\Delta f$  values.

Both waxes are impure compounds, although the AKD wax structure only differs slightly by the hydrocarbon chain length, whereas the CW consists of several different compounds. There appears to be different opinions in the literature regarding the exact structural makeup of CW, although it does change depending on its plant source and age of the plant (Wang et al. 2001; Puttalingamma 2014). The varieties of CW compounds shown in Fig. 2b are those determined by Wang et al. (Wang et al. 2001), where over 33 individual structures were identified through pyrolysis-GC measures and grouped into five different classes as drawn.

The different wax interactions with cellulose as explained for the SCI-treated papers also appears valid at the interfacial level. The hydrophobicity of nonannealed CW-treated papers showed little improvement in the CA, and the loose attachment of this complex compound to the cellulose interface may help explain its poor performance at the bulk level. Just over 50 mol% of CW contains the more electronegative=O groups that could attach to the -OH groups on cellulose. Since many of these groups may H-bond with other fractions within CW, the available = O groups is postulated at less than 50 mol%. The easy removal of much of the CW during the n-heptane flush therefore seems very plausible. The nonannealed AKD-treated papers showed excellent hydrophobic improvement with time, however the relatively long time to adequate sizing (approx. 14 days) seems to be mimicked by the long times to equilibrium at the interface. The vast improvement in bulk hydrophobicity is also likely linked to the much stronger attachments of the AKD to the cellulose fibers.

## Effects of wax concentration and temperature

The frequency signal is directly correlated to mass of solute adsorbed onto the sensor, particularly when Sauerbrey behavior is demonstrated as previously established. Therefore, changes in wax concentration should produce a similar ratio of change in the  $\Delta f$  signal. However, as observed in Fig. 6 and Table 1, other conditions such as temperature can also influence the quantity of solute adsorbed, which contribute to a change in the  $\Delta f$  signal.

Equilibration of the AKD signal was not possible at the concentrations initially studied (0.9 and 1.8 g/L) and hence a concentration of 0.45 g/L was subsequently tested. Although an improvement was noted, there was still a small additional adsorption recorded during a second AKD/n-heptane adsorption cycle (Fig. 6a). Barely any AKD was removed with n-heptane flushing, quantified between approximately 2 – 5% as per Table 1. For each doubling of



8000

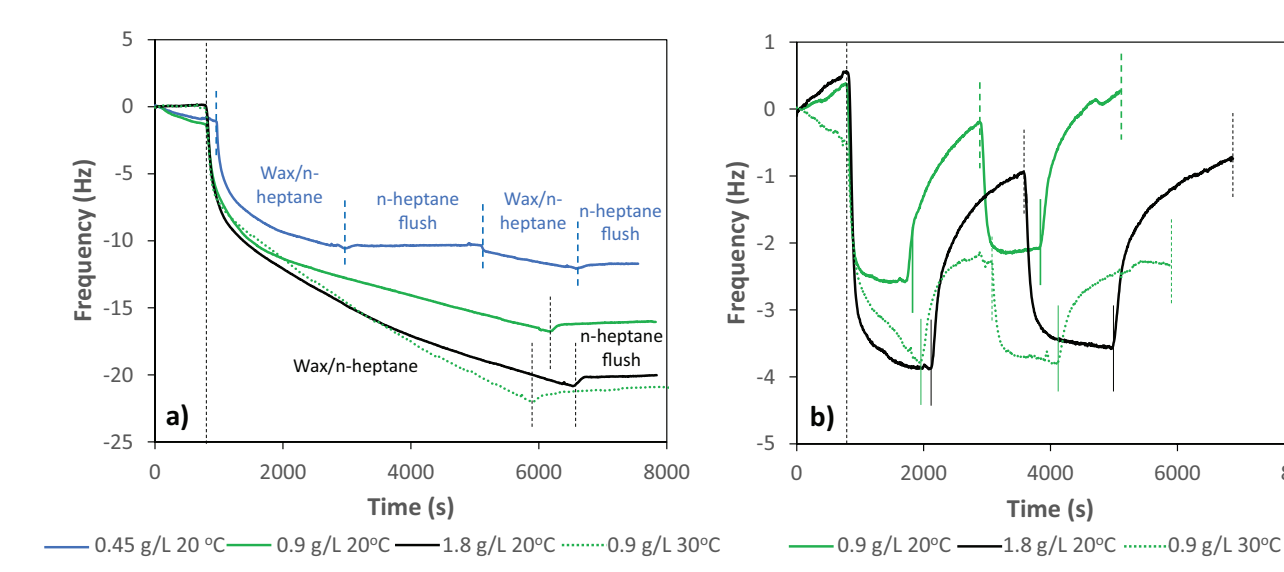


Fig. 6 a AKD and b CW adsorption onto cellulose-coated sensors, demonstrating changes with wax concentration and operating temperature. All traces shown are for the  $f_7$  overtone signal. In a), adsorption and flushing sections are identified. In

b), adsorption sections are between --- and — vertical lines; flushing is between - and --- vertical lines on each experimental curve

4000

Time (s)

6000

concentration tested, the resulting  $\Delta f$  values were approximately 1.5 times the original value instead of the expected 2 times higher.

The trial at 0.9 g/L was repeated at 30 °C, and is also plotted in Fig. 6a. There is a considerable increase in the quantity of AKD adsorbed from the wax/n-heptane solution at the higher temperature. The final value recorded is approximately the same that can be achieved at the higher concentration of 1.8 g/L. Similarly, only small quantities of adsorbed AKD wax could be removed during n-heptane flushing at the higher temperature. Experiments described

**Table 1** Absolute values of  $\Delta f$  (n=7) for AKD and CW adsorption to cellulose-coated SiO<sub>2</sub> sensors at the various conditions tested, together with the %-wax removed during in Fig. 1 demonstrate the vast improvement in AKD impregnated into cellulose substrates that were annealed, based on the much-improved CA on Days 1 and 7. Although the higher temperature QCM-D experiment was only 10 °C above room temperature conditions, this result demonstrates that the additional heat energy fosters enhanced adsorption of the AKD molecules at the cellulose interface.

Similar experimental trials shown in Fig. 6b and also quantified in Table 1 for CW tell a vastly different story. In Fig. 6b, the relative increase in  $\Delta f$  values for a doubling of CW concentration varied between

the n-heptane flush sequence. All frequency values are averaged over the last 90 s of each stage, and have a typical error of  $\pm 0.01$  Hz

Conditions	Wax/n-heptane adsorption (Hz)	% wax removed during n-heptane flush	Second wax/n-heptane adsorption (Hz)	% wax removed during second n-heptane flush	
AKD wax solute					
0.45 g/L; 20 °C	9.42	1.57	11.01	2.71	
0.9 g/L; 20 °C	14.76	4.21	Not attempted		
1.8 g/L; 20 °C	20.92	3.56			
0.9 g/L; 30 °C	21.59	4.83			
CW solute					
0.9 g/L; 20 °C	2.92	80.72	2.42	89.79	
1.8 g/L; 20 °C	4.38	65.68	4.08	68.33	
0.9 g/L; 30 °C	3.27	43.68	3.40	41.21	



1.5 times during the first adsorption stage to 1.7 during the second adsorption stage. While this is a little better than that demonstrated for the AKD experiments, it still falls short of the expected × 2 change in  $\Delta f$  values. At room temperature conditions (20 °C), between 80 – 90% of CW was removed at the lower CW concentration, while the higher concentration trial showed a 65 - 68% removal. More CW physically present in the higher concentration improved the chances of accessing more -OH groups on the cellulose. Since greater adsorption was possible between these functional groups, less of the CW was removed during the n-heptane flushing sequence. The quantity of CW removed is considerably greater than that for AKD regardless of concentration, and this issue may be viewed both positively and negatively. On the downside, this easy removal reduces its viability as a food-grade wax for hydrophobic packaging material development. However, its easy removal benefits packaging recycling – further investigations are needed that focus on ease of recyclability.

The trial performed at 0.9 g/L concentration and 30 °C also showed higher adsorption of CW wax, approximately matching that of the higher concentration trial at the lower temperature. The additional heat energy may have enabled a weakening of H-bonds between the CW fractions, freeing up the availability to H-bond to the cellulose instead. The quantity of CW removed during the n-heptane flush was reduced to half that recorded at room-temperature conditions, again showing stronger attachments of the wax to cellulose at these conditions.

Interfacial energy between the waxes and cellulose sensors

The spreadability of both wax preparations over cellulose substrates was briefly investigated based on Young's equation stated in Eq. (1). The uncoated SiO<sub>2</sub> QSense sensors had a roughness < 1 nm RMS (Biolin Scientific 2024). Spin-coating these surfaces with 1 wt% CNCs would have increased the roughness, but they were still assumed *notionally smooth* to validate use of Young's equation. In a similar manner, the coated surface was assumed non-porous, notwithstanding the reality that pore space between the CNCs clusters existed within the thickness of the coating itself. These assumptions are reasonable when compared with Whatman 1 filter paper, with

predicted porosity calculated at 17% (Cytiva 2024), and roughness of nanofibrillated cellulose films measured between 0.5 – 3.5 μm (Miettinen et al. 2014). [See Supplementary Information Online Resource 1 for porosity calculation]. Pendant drop measurements were performed for the 1.8 g/L concentration preparations for both waxes, and results are shown in Table 2. Surface measurements and calculations show that both wax/n-heptane solutions behave similarly in their spreading capabilities across *smooth* cellulose surfaces, with relatively low surface tensions, very low CA, and low interfacial tensions, indicating high spreading across the fibers.

## Adsorption kinetics of AKD and CW onto cellulose

The previous discussion mostly relied on qualitative observations from the QCM-D studies to draw significant observations regarding the different behavior of each wax at the interface with the cellulose-coated substrates. A quantitative assessment of the adsorption kinetics is now addressed. The overtone number, n=7, was used in Eq. (4) to convert frequency values to mass values of the waxes adsorbed (or desorbed) onto (from) the cellulose surface.

## AKD adsorption kinetics analysis

The best fits of data for each trial was the summation of three PFO equations:

$$q_t = q_{e,1} (1 - e^{-r_1 t}) + q_{e,2} (1 - e^{-r_2 t}) + q_{e,3} (1 - e^{-r_3 t})$$
(5)

In Eq. (5),  $q_t$  and t have been previously defined;  $q_{e,1}$ ,  $q_{e,2}$ ,  $q_{e,3}$ , are the 'equilibrium' quantities adsorbed (ngcm<sup>-2</sup>) within each sub-section;  $r_1$ ,  $r_2$ ,  $r_3$ , are the first-order rate constants (s<sup>-1</sup>) relating to each sub-section. Intuitively,  $\sum_{i=1}^{i=3} q_{e,i} = q_e$ , since together

**Table 2** Results of pendant droplet studies to determine the interfacial energies between wax/n-heptane solutions and cellulose substrates using Eq. (1). Surface energy of cellulose,  $\sigma_{\rm SV}$ , obtained from (Gamelas 2013)

Wax/n- heptane solution, 1.8 g/L	$\sigma_{ m LV}~{ m mNm^{-1}}$	$\sigma_{\rm SV}~{ m mNm^{-1}}$	θ ο	$\sigma_{\rm SL}~{\rm mNm^{-1}}$
AKD	$29.4 \pm 0.3$	43.7	$2.3 \pm 0.4$	14.3

43.7

 $4.2 \pm 0.2$  13.4

 $30.4 \pm 0.6$ 

CW



**Table 3** Fitted constants for AKD adsorption kinetic studies using Eq. (5). All quantities, q, have units ngcm<sup>-2</sup>, while all rate constants, r, have units s<sup>-1</sup>

Conditions	$q_{e,1}$	$r_1$	$q_{e,2}$	$r_2$	$q_{e,3}$	$10^4 * r_3$	$q_e$	SD
0.45 g/L; 20 °C	5.918	0.04442	7.806	0.005075	11.55	8.492	25.27	1.75
0.9 g/L; 20 °C	10.19	0.01243	12.57	0.001434	-	0.002799	-	1.75
1.8 g/L; 20 °C	16.17	0.01406	3.184	0.002995	41.86	2.482	61.21	1.01
0.9 g/L; 30 °C	5.396	0.02545	10.30	0.01406	61.43	1.906	77.13	2.88

the total quantity of wax adsorbed should equal the sum of that adsorbed within each sub-section, provided that each individual section reached its own equilibrium.

While Eq. (5) is clearly empirical, it follows similar logic to that used by Shen et al. (Shen et al. 2015) where obvious changes in rate constant were identified by sudden changes in gradient of the  $\Delta f$  (or  $\Delta m$ ) curves. This form may also describe the three mass transfer stages known to occur in adsorption processes: a) external diffusion of the adsorbate (wax) through the liquid film (solvent/cosolvent) to the adsorbent (cellulose fibers); b) internal diffusion of the wax into the pores between the cellulose fibers; and c) adsorption of the wax onto active sites on the cellulose (Wang and Guo 2020).

The fitted constants from Eq. (5) have been summarized in Table 3 for AKD adsorption kinetic trials at the various experimental conditions indicated. No desorption processes were considered since very little AKD was removed during the n-heptane flushing sequence. Examples of the fitted data are shown in Fig. 7a and b. The raw data for all conditions (in frequency) is shown in Fig. 6a, and it can be seen that the curve for 0.9 g/L, 20 °C did not show any signs of coming to equilibrium, despite good mathematical fits obtained for this data. Consequently, there were issues in reporting the  $q_{e,3}$  value, and the  $r_3$  value was also considerably lower than those determined for the other experimental conditions. From Table 2, it can be seen that  $r_1 > r_2 > r_3$  across all conditions tested. In most cases, the orders of magnitude for these three rate constants were  $10^{-2}$ ,  $10^{-3}$ , and  $10^{-4}$  respectively (two exceptions only). If it is assumed that the three-step mass transfer process is represented by the three PFO expressions making up Eq. (6), then the external diffusion of the AKD through

the n-heptane towards the cellulose surface was the quickest step. Likewise, the intermediate step was the AKD working its way through the cellulose fiber pores, and the rate-limiting step was the AKD attaching to the cellulose via H-bonding (Adenekan and Hutton-Prager 2019). The  $q_e$  values were all somewhat higher than the experimental  $q_{\rho}$ values obtained, as shown in Fig. 7a and b where none of the conditions reached equilibrium due to the slow, rate-limiting step. Higher operating temperatures (i.e. 30 °C compared with 20 °C) noticeably increased the mass transfer of the wax through the cellulose fiber pores  $(r_2)$ . Lower AKD concentrations (0.45 g/L compared with 0.9 and 1.8 g/L) noticeably increased all three mass transfer steps. Less wax within the n-heptane solvent meant that individual wax molecules could more easily migrate towards the cellulose surface and into the pores. Lower concentration also meant there was less competition for the individual molecules to find and attach to the active sites on the cellulose.

## CW adsorption kinetics analysis

The CW adsorption kinetics demonstrated quite different behavior from the AKD kinetics. Due to faster equilibration times, substantial desorption of CW during n-heptane flushing sequences, and the ability to run a second adsorption and flushing sequence during the same trial, both adsorption and desorption stages were considered. The adsorption of CW onto cellulose was modeled via a single PFO equation as shown in Eq. (2). Desorption was modeled using the summation of two first-order equations, as shown in Eq. (6) (Fang et al. 2020):

$$q_t = q_{e,1}e^{-r_1t} + q_{e,2}e^{-r_2t} (6)$$



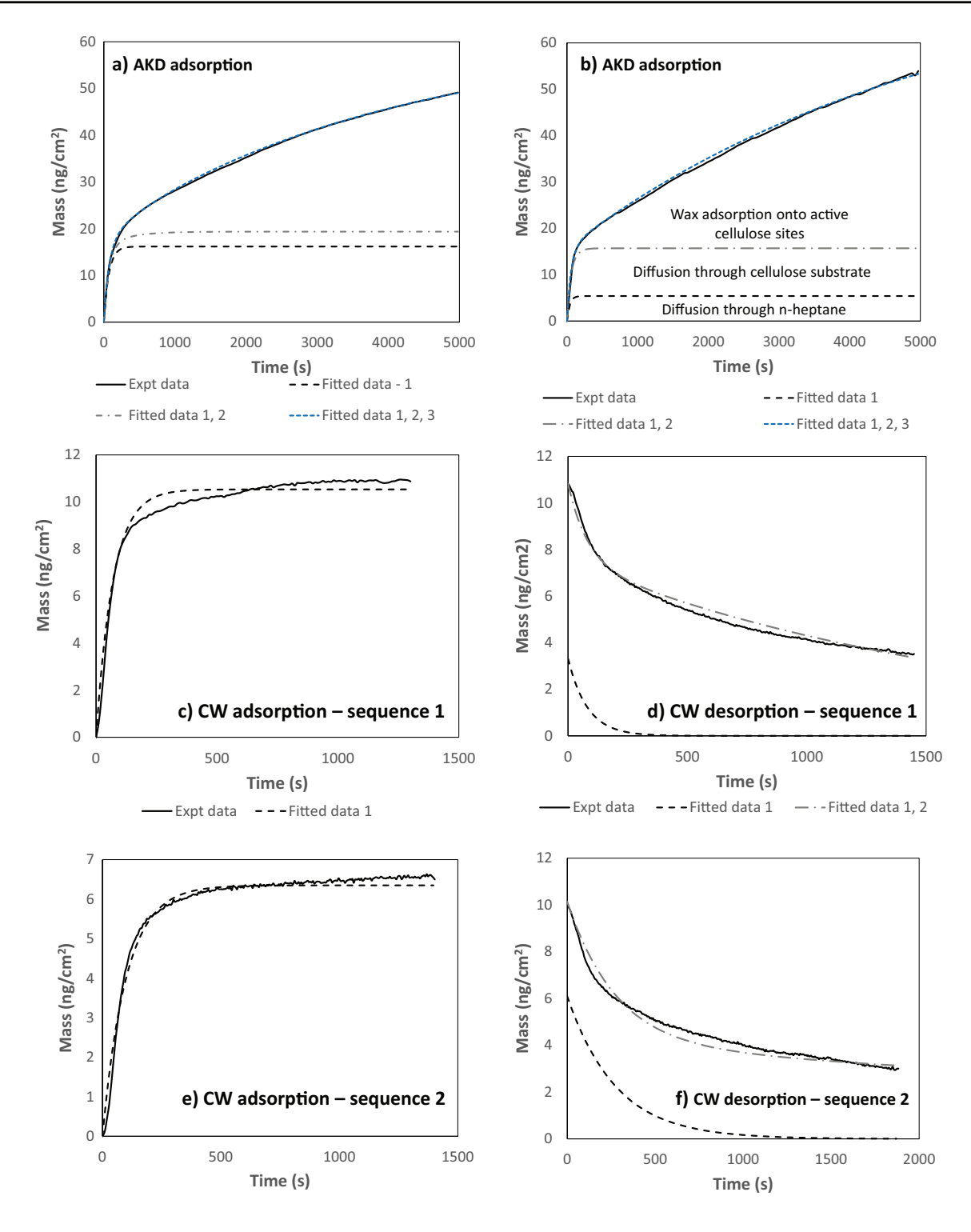


**Fig. 7** Examples of fitted equations to the experimental data, converted from frequency to mass using Eq. (4). **a** AKD data at 1.8 g/L, 20 °C, and **b** AKD at 0.9 g/L, 30 °C, showing the three fitted portions making up the overall experimental curve.

CW at 1.8 g/L, 20 °C first adsorption/flushing sequence, showing  $\bf c$  the single PFO fitted equation for the adsorption, and  $\bf d$  the double fitted equation for the desorption.  $\bf e$  and  $\bf f$  show the same CW trial but for the second adsorption/flushing sequence



The symbols in Eq. (6) have similar meaning as described for Eq. (5), except that the equilibrium quantities now refer to the amount of wax *desorbed* in each sub-section, and the rates are *desorption* rate constants instead of adsorption rate constants. Units for both quantities remain the same. As with Eq. (5), the expression in Eq. (6) represents two clear stages identified during the desorption process. The raw data for each CW condition are shown in Fig. 6b, and due to the unusualness of the first adsorption/desorption stage in the 30 °C trial, only the second stage was analyzed. Examples of the fitted equations with the data are shown in Fig. 7c - f.

Fitted rate constants are shown in Table 4 for CW. In all adsorption cases (both first and second sequences during the trial), the rate constant  $k_1$ approximated to  $10^{-2}$  s<sup>-1</sup>, irrespective of temperature or CW concentration. This is the same order of magnitude as  $r_1$  in the AKD adsorption analysis, and may indicate that the dominant mass transfer for CW adsorption was only the external diffusion of wax to the cellulose surface. This apparent single-step mass transfer to the surface may also be in keeping with the fact that CW was easily washed off during the n-heptane flush. It may also indicate that the CW had not substantially diffused through the cellulose pores or firmly attached to active sites on the cellulose itself. Although two- and three-step PFO equations in keeping with Eq. (5) were tried, there was little improvement in the overall fit. Note also that the SD represents data points after the first 30-40 s for each adsorption trial, due to the lack of fit in the initial time period. One of the main reasons that the initial kinetics were less accurately modeled with the

**Table 4** Fitted constants for CW adsorption and desorption kinetic studies using Eqs. (2) and (6). All quantities, q, have units  $ngcm^{-2}$ , while all rate constants, r or k, have units  $s^{-1}$ . '1' refers to the first sequence of CW/n-heptane adsorption and

CW trials was the presence of a small lag-time before the adsorption rate significantly increased.

The desorption analysis showed more variation among different experimental conditions with the values of both rate constants, but the emerging consistent pattern was that  $r_1 > r_2$ . The higher temperature condition at 30 °C had lower desorption rates than the 20 °C trial at the same concentration by one and two orders of magnitude respectively for the two rate constants  $(r_1 \text{ and } r_2)$ . This is likely explained by the significantly lower quantities of CW removed at the higher temperature, resulting in slower desorption rates. The sum of the individual q's,  $q_{e,total}$ , matched the initial starting quantity of CW in all desorption cases. The two stages within the desorption process resulting in fitted values for  $r_1$  and  $r_2$  are not easily explainable, particularly given that only one major step was identified during the adsorption process. One plausible explanation could be a fast, initial removal of excess CW simply lying on the cellulose surface, followed by a slower removal of CW that had partially oriented onto the active sites for cellulose attachment. This desorption process warrants further investigation.

# Other fitted equations

Raw data for both waxes were fitted with the PSO equation (Eq. (3)), where  $t/q_t$  was plotted against t. If PSO behavior was observed, then a straight line would result with gradient of  $1/q_e$  and intercept of  $1/k_2q_e^2$ . Curved lines resulted with the AKD data, which became more pronounced as both the concentration and temperature increased. Hence, AKD was better-represented with

n-heptane flushing process, while '2' refers to the subsequent sequence of adsorption/flushing over the same sensors.  $q_{e,total}$  refers to the summation of  $q_{e,1}$  and  $q_{e,2}$  for the desorption process only

Conditions	$q_e$	$k_1$	$q_{e,1}$	$r_{I}$	$q_{e,2}$	$10^4 * r_2$	$q_{e,total}$	SD
	Adsorption 1		Desorptio	n 1		,		
0.9 g/L; 20 °C	7.229	0.01517	3.549	0.003819	3.594	9.791	7.143	5.41
1.8 g/L; 20 °C	10.53	0.01427	3.318	0.01230	7.505	5.555	10.82	4.38
0.9 g/L; 30 °C	Not attempted		Not attem	pted				-
	Adsorption 2		Desorptio	Desorption 2				
0.9 g/L; 20 °C	4.669	0.01634	0.1024	0.01119	2.912	28.65	3.014	7.46
1.8 g/L; 20 °C	6.096	0.009958	6.096	0.01081	4.046	4.112	10.14	5.93
0.9 g/L; 30 °C	3.708	0.01522	3.708	0.003233	4.727	0.5543	8.435	3.81



PFO equations. Only the adsorption curves were fitted for CW conditions, and most showed relatively straight lines after an initial minimum at early times. There were also difficulties fitting the initial time data with the PFO equation, however, even removing these early data from the PSO analysis, the minimum still existed. It is possible that the CW adsorption process followed PSO behavior at later times, but as noted by Wang and Guo (Wang and Guo 2020), kinetics data near equilibrium at later times tended to bias the PSO model. The majority of kinetic data producing the straight line in the PSO assessment fell into this category. The Ritchie model was also considered, but as it is essentially the same as the PFO and PSO models at low values of the fitting parameter (n'=1 or 2), no further attempts were made. More investigation is needed with this wax, but at this stage, the PFO model was the most suitable fit that could be found.

#### **Conclusions and Recommendations**

This study has made direct links between interfacial behavior and bulk property improvements for the case of supercritically impregnated paper substrates with hydrophobic wax solutes. The bulk paper study showed immediate hydrophobic improvements to the paper with heat treatment (4 h, 140 °C) for both waxes, and also that AKD wax provided considerably more hydrophobicity than CW, even without heat treatment. The interfacial study demonstrated a slow but strong deposition of AKD onto the Whatman cotton lint fibers. All three classic mass transfer processes of adsorption were observed, and the slowest step (AKD attachment onto cellulose active sites) was indicative of the slow bulk hydrophobic improvement in AKD-treated samples. More rapid deposition observed at higher temperatures also mimicked the immediate development of bulk hydrophobicity with annealing. Equivalently, CW, which showed only mild hydrophobic development with heat and none at all without heat in CW-treated papers, underwent only the first mass transfer process at the interface and was easily removed. The vast differences in chemical structure and purity were also thought to contribute (positively and negatively) to the attachment ability of the waxes onto the cellulose.

These results are believed to be the first attempt at explaining bulk property development of supercritically treated paper via interfacial investigations. There are only a handful of QCM-D interfacial studies with AKD in relation to papermaking (Kallio et al. 2004; Nypelö et al. 2011), none of which are associated with SCI processes. There are no reported studies of CW in relation to interfacial studies on any surface. Future investigations will extend this work to optimize interfacial adsorption kinetics and molecular bonding to influence bulk paper properties; investigate realistic paper substrates to quantify more complex interactions taking place between solute and substrate; and study desorption kinetics to further develop sustainable and recyclable packaging.

**Author contributions** Dr. Hutton-Prager: Conceptualization, Methodology, Formal analysis, Investigation, Resources, Writing – Original Draft and Review & Editing, Visualization, Supervision, Project administration, Funding acquisition. Mr. Fallon: Methodology, Validation, Investigation. Mr. Henke: Methodology, Investigation, Formal analysis. Mr. Zhang: Investigation. Ms. Perera: Investigation.

**Funding** QCM-D data and analysis is supported by MRI NSF grant #2018004. Funding for undergraduate student and co-author Blake Henke was provided by the NSF REU Site: Ole Miss Nanoengineering Summer REU Program (NSF ENG/EEC #2148764). Funding by high school student and co-author Raymond Zhang was provided by the ARISE@UM program, and in part through the auspices of the ARISE MS Foundation and NSF grants #2120084 and #1846376. Funding for graduate student Keshani Perera was provided by NSF grant #2322501.

#### **Declarations**

Ethical approval Not applicable.

**Competing interests** The authors have no relevant financial or non-financial interests to disclose.

**Open Access** This article is licensed under a Creative Commons Attribution 4.0 International License, which permits use, sharing, adaptation, distribution and reproduction in any medium or format, as long as you give appropriate credit to the original author(s) and the source, provide a link to the Creative Commons licence, and indicate if changes were made. The images or other third party material in this article are included in the article's Creative Commons licence, unless indicated otherwise in a credit line to the material. If material is not included in the article's Creative Commons licence and your intended use is not permitted by statutory regulation or exceeds



the permitted use, you will need to obtain permission directly from the copyright holder. To view a copy of this licence, visit http://creativecommons.org/licenses/by/4.0/.

#### References

- Adamczyk Z, Pomorska A, Sadowska M et al (2022) QCM-D Investigations of Anisotropic Particle Deposition Kinetics: Evidences of the Hydrodynamic Slip Mechanisms. Anal Chem 94:10234–10244. https://doi.org/10.1021/acs.analchem.2c01776
- Adenekan K, Hutton-Prager B (2019) Sticky hydrophobic behavior of cellulose substrates impregnated with alkyl ketene dimer (AKD) via sub- and supercritical carbon dioxide. Colloids Surf, A 560:154–163. https://doi.org/10.1016/j.colsurfa.2018.09.073
- Adenekan K, Hutton-Prager B (2020) Modeling the solubility of Alkyl Ketene Dimer in supercritical carbon dioxide: Peng-Robinson, group contribution methods, and effect of critical density on solubility predictions. Fluid Phase Equilib 507:112415. https://doi.org/10.1016/j.fluid.2019.112415
- Beheshtimaal A, Hutton-Prager B (2022) Exploring the relationship between food-grade wax solubility in supercritical carbon dioxide and resulting hydrophobic development of impregnated paper substrates. Colloids Surf, A 654:130134. https://doi.org/10.1016/j.colsurfa.2022.130134
- Brock T, Groteklaes M, Mischke P (2010) European Coatings Handbook, 2nd rev edn. Vincentz Network, Hannover Germany. ISPN 978-3-86630-849-7
- Chen Q, Xu S, Liu Q et al (2016) QCM-D study of nanoparticle interactions. Adv Coll Interface Sci 233:94–114. https://doi.org/10.1016/j.cis.2015.10.004
- Chen S, Song Y, Xu F (2018) Highly Transparent and Hazy Cellulose Nanopaper Simultaneously with a Self-Cleaning Superhydrophobic Surface. ACS Sustain Chem Eng 6:5173–5181. https://doi.org/10.1021/acssuschemeng.7b04814
- Cui M, Duan Y, Ma Y et al (2020) Real-Time QCM-D Monitoring of the Adsorption-Desorption of Expansin on Lignin. Langmuir 36:4503–4510. https://doi.org/10.1021/acs.langmuir.0c00104
- Cytiva (2024) A Guide to Whatman Filter Paper Grades. https://www.cytivalifesciences.com/en/us/solutions/lab-filtration/knowledge-center/a-guide-to-whatman-filter-paper-grades. Accessed 16 Jan 2024
- Di Risio S, Yan N (2006) Characterizing coating layer z-directional binder distribution in paper using atomic force microscopy. Colloids Surf, A 289:65–74. https://doi.org/10.1016/j.colsurfa.2006.04.007
- Dourado AHB, Silva RA, Torresi RM et al (2018) Kinetics, Assembling, and Conformation Control of L-Cysteine Adsorption on Pt Investigated by in situ FTIR Spectroscopy and QCM-D. ChemPhysChem 19:2340–2348. https://doi.org/10.1002/cphc.201800380
- Easley AD, Ma T, Eneh CI et al (2022) A practical guide to quartz crystal microbalance with dissipation monitoring of thin polymer films. J Polym Sci 60:1090–1107. https://doi.org/10.1002/pol.20210324
- Fang D, Zhuang X, Huang L et al (2020) Developing the new kinetics model based on the adsorption process: From fitting

- to comparison and prediction. Sci Total Environ 725:138490. https://doi.org/10.1016/j.scitotenv.2020.138490
- FDA (2024a) Title 21--food and drugs chapter i--food and drug administration department of health andhuman services subchapter B food for human consumption (continued) part 184 -- direct foodsubstances affirmed as generally recognized as safe subpart B listing of specific substances affirmed as GRAS. https://www.accessdata.fda.gov/scripts/cdrh/cfdocs/cfcfr/CFRSearch.cfm?fr=184.1978. Accessed 26 June 2024
- FDA (2024b) Title 21--food and drugs chapter i--food and drug administration department of health andhuman services subchapter B food for human consumption (continued) part 176 -- indirect foodadditives: paper and paperboard components subpart B substances for use only as components of paperand paperboard. https://www.accessdata.fda.gov/scripts/cdrh/cfdocs/cfCFR/CFRSearch.cfm?fr= 176.120. Accessed 26 June 2024
- Franco P, De Marco I (2020) Supercritical Antisolvent Process for Pharmaceutical Applications: A Review. Processes 8:938. https://doi.org/10.3390/pr8080938
- Gamelas JAF (2013) The surface properties of cellulose and lignocellulosic materials assessed by inverse gas chromatography: a review. Cellulose 20:2675–2693. https://doi.org/10.1007/s10570-013-0066-5
- Howard KW, Hodgson KT (2015) Influence of pigment packing behavior on the adhesive requirements of aqueous paper coatings. J Coat Technol Res 12:237–245. https://doi.org/10.1007/s11998-014-9645-0
- Hu Q, Wang Q, Feng C et al (2018) Insights into mathematical characteristics of adsorption models and physical meaning of corresponding parameters. J Mol Liq 254:20–25. https://doi.org/10.1016/j.molliq.2018.01.073
- Hutton BH, Parker IH (2008) Immediate consolidation behaviour of aqueous pigment coatings applied to porous substrates. Chem Eng Sci 63:3348–3357. https://doi.org/10.1016/j.ces.2008.03.039
- Hutton-Prager B, Adenekan K, Sypnewski M et al (2021) Hydrophobic development and mechanical properties of cellulose substrates supercritically impregnated with food-grade waxes. Cellulose 28:1633–1646. https://doi.org/10.1007/s10570-020-03628-2
- Kallio T, Kekkonen J, Stenius P (2004) The formation of deposits on polymer surfaces in paper machine wet end. J Adhes 80:933–969. https://doi.org/10.1080/00218460490508742
- Kiran E (2016) Supercritical fluids and polymers The year in review 2014. J Supercrit Fluids 110:126–153. https://doi.org/10.1016/j.supflu.2015.11.011
- Kumar S, Chauhan VS, Chakrabarti SK (2016) Separation and analysis techniques for bound and unbound alkyl ketene dimer (AKD) in paper: A review. Arab J Chem 9:S1636–S1642. https://doi.org/10.1016/j.arabjc.2012.04.019
- Kumar R, Thakur AK, Banerjee N, Chaudhari P (2021) A critical review on the particle generation and other applications of rapid expansion of supercritical solution. Int J Pharm 608:121089. https://doi.org/10.1016/j.ijpharm. 2021.121089
- Lambourne R (1999) Paint composition and applications a general introduction. In: Lambourne R, Strivens TA (eds) Paint and Surface Coatings Theory and Practice, 2nd edn. Woodhead Publishing Ltd, Cambridge England, pp 1–18



- Medina SC, Farinha ASF, Emwas A-H et al (2020) A fundamental study of adsorption kinetics of surfactants onto metal oxides using quartz crystal microbalance with dissipation (QCM-D). Colloids Surf, A 586:124237. https://doi.org/10.1016/j.colsurfa.2019.124237
- Miettinen A, Chinga-Carrasco G, Kataja M (2014) Three-Dimensional Microstructural Properties of Nanofibrillated Cellulose Films. IJMS 15:6423–6440. https://doi.org/10. 3390/ijms15046423
- Misra SK, Pathak K (2020) Supercritical fluid technology for solubilization of poorly water soluble drugs via micro-andnaonosized particle generation. ADMET & DMPK 8(4):355–374. https://doi.org/10.5599/admet.811
- Mohamed AMA, Abdullah AM, Younan NA (2015) Corrosion behavior of superhydrophobic surfaces: A review. Arab J Chem 8:749–765. https://doi.org/10.1016/j.arabjc.2014.03.006
- Nechita P, Roman M (2020) Review on Polysaccharides Used in Coatings for Food Packaging Papers. Coatings 10:566. https://doi.org/10.3390/coatings10060566
- Nypelö T, Osterberg M, Zu X, Laine J (2011) Preparation of ultrathin coating layers using surface modified silica nanoparticles. Colloids Surf, A 392:313–321. https://doi.org/10.1016/j.colsurfa.2011.10.009
- Puttalingamma V (2014) Edible Coatings of Carnauba Wax A Novel Method For Preservation and Extending Longevity of Fruits and Vegetables A Review. Internet Jo Food Saf 16:1–5
- Quan C, Werner O, Wagberg L, Turner C (2009) Generation of superhydrophobic paper surfaces by a rapidly expanding supercritical carbon dioxide-alkyl ketene dimer solution. J Supercrit Fluids 49:117–124. https://doi.org/10.1016/j. supflu.2008.11.015
- Rossmann M, Braeuer A, Leipertz A, Schluecker E (2013) Manipulating the size, the morphology and the polymorphism of acetaminophen using supercritical antisolvent (SAS) precipitation. J Supercrit Fluids 82:230–237. https://doi.org/10.1016/j.supflu.2013.07.015
- Santos S, Puna J, Gomes J (2022) A Brief Review of the Supercritical Antisolvent (SAS) Technique for the Preparation of Nanocatalysts to Be Used in Biodiesel Production. Energies 15:9355. https://doi.org/10.3390/en15249355
- Biolin Scientific (2024) QSense Sensors. https://www.biolinscientific.com/qsense/sensors. Accessed 19 Jan 2024

- Shen D, Ma X, Cai T et al (2015) Investigation on kinetic processes of zeolitic imidazolate framework-8 film growth and adsorption of chlorohydro-carbons using a quartz crystal microbalance. Anal Methods 7:9619–9628. https://doi.org/10.1039/C5AY02188J
- Teixeira Moutinho IM, Kleen AM, Lopes Figueiredo MM, Tavares Ferreira PJ (2009) Effect of surface sizing on the surface chemistry of paper containing eucalyptus pulp. hfsg 63:282–289. https://doi.org/10.1515/HF.2009.046
- Tracton AA (ed) (2007) Coatings materials and surface coatings. CRC Press, Boca Raton, Fla
- Wang J, Guo X (2020) Adsorption kinetic models: Physical meanings, applications, and solving methods. J Hazard Mater 390:122156. https://doi.org/10.1016/j.jhazmat. 2020.122156
- Wang L, Ando S, Ishida Y et al (2001) Quantitative and discriminative analysis of carnauba waxes by reactive pyrolysis-GC in the presence of organic alkali using a vertical microfurnace pyrolyzer. jaap 58–59:525–537
- Wang Y, Zhang X, Kan L et al (2022) All-biomass-based ecofriendly waterproof coating for paper-based green packaging. Green Chem 24:7039–7048. https://doi.org/10.1039/ D2GC02265F
- Werner O, Turner C (2012) Investigation of different particle sizes on superhydrophobic surfaces made by rapid expansion of supercritical solution with in situ laser diffraction (RESS-LD). J Supercrit Fluids 67:53–59. https://doi.org/10.1016/j.supflu.2012.03.008
- Werner O, Quan C, Turner C et al (2010) Properties of superhydrophobic paper treated with rapid expansion of supercritical CO2 containing a crystallizing wax. Cellulose 17:187–198. https://doi.org/10.1007/s10570-009-9374-1
- Zhang W, Lu P, Qian L, Xiao H (2014) Fabrication of superhydrophobic paper surface via wax mixture coating. Chem Eng J 250:431–436. https://doi.org/10.1016/j.cej.2014.04.050

**Publisher's Note** Springer Nature remains neutral with regard to jurisdictional claims in published maps and institutional affiliations.

